Comparative study of Cl_2, Cl_2/O_2, and Cl_2/N_2 inductively coupled plasma processes for etching of high-aspect-ratio photonic-crystal holes in InP

C. F. Carlström[a] and R. van der Heijden[b]
COBRA Research Institute and Center for NanoMaterials, Eindhoven University of Technology, P.O. Box 513, NL 5600 MB Eindhoven, The Netherlands

M. S. P. Andriesse
Kavli Institute of Nanoscience, Delft University of Technology, P.O. Box 5053, 2600 GB Delft, The Netherlands

F. Karouta and R. W. van der Heijden[c]
COBRA Research Institute and Center for NanoMaterials, Eindhoven University of Technology, P.O. Box 513, NL 5600 MB Eindhoven, The Netherlands

E. van der Drift
Kavli Institute of Nanoscience, Delft University of Technology, P.O. Box 5053, 2600 GB Delft, The Netherlands

H. W. M. Salemink
COBRA Research Institute and Center for NanoMaterials, Eindhoven University of Technology, P.O. Box 513, NL 5600 MB Eindhoven, The Netherlands and Kavli Institute of Nanoscience, Delft University of Technology, P.O. Box 5053, 2600 GB Delft, The Netherlands

(Received 10 March 2008; accepted 10 July 2008; published 5 September 2008)

An extensive investigation has been performed on inductively coupled plasma etching of InP. An important motivation for this work is the fabrication of high-aspect-ratio holes for photonic crystals. The essential chemistry is based on Cl_2 with the addition of N_2 or O_2 for sidewall passivation. The influence of different process parameters such as gas flows, temperature, pressure, ion energy, and inductively coupled plasma power on the hole geometry is presented. It is concluded that photonic crystals can be etched with Cl_2 only; however, temperature and pressure control is critical. Adding passivation gases largely broadens the window in the parameter space for hole etching. Most importantly, etching of narrow holes can be carried out at higher temperatures where the etching is mass limited and spontaneous etching of InP by Cl_2 occurs.
 [DOI: 10.1116/1.2968696]

I. INTRODUCTION

Photonic crystals (PC) are already present in some of today's optical devices. Their use is likely to increase in the future since they allow for better performance and downscaled size. In particular, for operation at the telecommunication wavelength of 1550 nm, the InP material system is needed to include active devices such as lasers. A planar photonic crystal in InP typically consists of a two-dimensional (2D) triangular lattice of etched holes with a lattice constant of ~400 nm and a diameter of ~250 nm. To fulfill the requirement of low optical loss, the holes should be etched through an InP/InGaAsP/InP planar waveguide structure with sufficient depth and with smooth and vertical sidewalls.[1,2] In particular, the region close to the guiding layer should be vertical to reduce out-of-plane scattering.[1] For a typical waveguide structure, with a 500 nm InP cap layer on top of a 500 nm InGaAsP layer grown lattice matched on InP, this implies that the topmost 1.5–2 μm of the holes must be cylindrical.

Much effort has been devoted in the past to study reactive ion etching (RIE) of InP. Predominantly chlorine is used as the main chemically active species, which requires operation at elevated temperatures, around 200 °C, to obtain sufficient volatility for the reaction product $InCl_x$. Particularly, high-density plasma etching, using electron cyclotron resonance (ECR) or inductively coupled plasma (ICP) reactors, has been found to be very important for etching high-aspect-ratio features with smooth surface morphology. This method was used to realize large diameter ($\geqslant$10 μm) via holes with aspect ratio in the range of 1 (Ref. 3) to 3.[4] Even much higher aspect ratios ($\gtrsim$5) were obtained in narrow one-dimensional trenches for photonic devices with widths δ of 0.4 μm (Ref. 5) or ~0.3 μm.[6] Also, high-aspect 2D structures in the form of ~1-μm-diameter posts with a wide separation have been reported.[7]

Anisotropic dry etching of high-aspect-ratio structures suffers from feature-size-dependent etch depth, so-called RIE lag, which also strongly depends on dimensionality in

[a]Present address: QuNano AB, Lund, Sweden.
[b]Present address: ASML, P.O. Box 324, 5500AH Veldhoven, The Netherlands.
[c]Electronic mail: r.w.v.d.heijden@tue.nl

the plane, i.e., 2D or three dimensional. These effects become particularly severe when holes are etched with diameters well below 1 μm, where wide holes are etched deeper than narrow holes.[8] Even for the one-dimensional trenches, the effects are already strong when the transport of neutral species to the bottom of the hole is governed by Knudsen transport.[9] As a direct consequence, the delicate balance between ion and radical fluxes changes over the etch depth. For the regimes of deeply etched photonic crystals with hole diameters of ~200 nm and aspect ratios well above 10, new etching regimes must be explored. To keep anisotropy, it requires the highest control of the sidewall integrity, notably by sidewall passivation using smart gas additives like oxygen and nitrogen.

The best deeply etched photonic-crystal holes in InP have so far been produced by chlorine-based dry etching where the reactive Cl_2 gas was injected external to the plasma chamber in a directed ion flux.[10,11] Also in this chemically assisted ion-beam-etching (CAIBE) technique, the etch depths strongly depend on hole diameter for diameters well below 1 μm, as was shown in a recent systematic investigation.[12]

Successful etching of deep photonic-crystal holes has also been accomplished by high-plasma-density RIE using ECR (Ref. 13) or its modern replacement, ICP.[14] Processes using ICP reactors are highly relevant as they tend to be more abundantly present than CAIBE reactors. The reactive chlorine species were introduced either in the form of $SiCl_4$ gas[14] or of Cl_2 gas, as in our previous study.[15] We previously presented ICP etching processes using gas flow consisting either solely of Cl_2 or with the addition of N_2 or O_2 for sidewall passivation for the fabrication of deeply etched hole-type photonic crystals in the InP-based material system.[15–17] Very recently, a detailed study was presented on the use of N_2 as a passivation component in ICP etching of InP photonic crystals.[18] In the present article, we describe a comprehensive investigation of these processes and their conditions. Apart from the detailed report on using O_2 as the passivating component, a comparison of the use of O_2 and N_2 is also provided. Temperature is known to have a strong effect on Cl_2 dry etching, with etch rates being thermally activated.[19–21] Therefore, special attention is given to the sample temperature, which in ICP etching may be significantly higher than the set temperature of the table due to heating by the ion bombardment.[22] To study the influence of the carrier material on the etching, both Si and InP carrier wafers were used.

II. EXPERIMENT

Unless otherwise mentioned, all experiments were performed on (100) *n*-type InP (Sn-doped) substrates with a size of approximately 8×8 mm^2. The photonic-crystal pattern was defined into a layer of ZEP520A (positive electron-beam resist) with electron-beam lithography and then transferred into a 400-nm-thick plasma enhanced chemical vapor deposition deposited SiN_x-mask layer using a CHF_3-RIE process. After the final ICP etch step, the samples were cleaved and the cross section was inspected in a scanning electron microscope (SEM). From the SEM inspection, hole depths were determined, while large-area etch rates were measured with a profilometer. The ICP etch experiments were carried out in a load-locked Oxford Plasmalab 100 system. Since the main etch product, $InCl_3$, is not sufficiently volatile at room temperature, etching was performed at elevated temperatures (60–300 °C) using resistive heating. To keep the sample temperature as close as possible to the preset temperature of the table, the sample was glued with a heat-conducting paste (Dow Corning 340) onto a 4 in. carrier wafer. Thermal contact between the carrier wafer and table was established by He gas backflow. However, He leaked into the chamber with a leak rate of a similar magnitude as the process gas flow when working in the 1–2 mtorr pressure regime. Therefore, gas flows were maximized for a given pressure to keep He partial pressure at a minimum. Unfortunately, the leak rate depended on the mounting of the carrier wafer and also changed when the plasma was turned on, which made it impossible to predict the exact leak rate into the chamber. The substrate chuck temperature was measured with a thermocouple, and the carrier temperature was measured with thermo strips (Testo). The ion energy was controlled by the dc-bias voltage. Ion-current density was measured using a Langmuir probe.

III. SUBSTRATE TEMPERATURE

The temperature of the sample was evaluated using the three main thermal contributions: (a) plasma-heating power, (b) radiation loss from the carrier to the environment, and (c) heat loss from the carrier down to the substrate table (see Fig. 1). Actual calculations were done in the finite element approach using the FEMLAB® program (from COMSOL AB, Sweden). The heating power from the plasma to the carrier wafer was measured by comparing temperature versus power relations from constant table heating powers with those when the plasma was the only heating source. This comparison was performed for all studied plasma processes. This is similar to the method described by Sabin.[22] The geometry for heat radiation is approximated as two parallel plates with emissivity $\varepsilon=0.03$. With the chamber wall temperature together with the geometrical parameters and the heat conductivities of Si, InP, and glue[23] known, a heat-transfer constant h between the carrier and the table could be obtained by fitting the model to the experimental data. This, in turn, allowed for the maximum sample temperature to be estimated, and it was found to be 2–5 °C higher than the carrier temperature for heating-power densities ranging from 1–2 W cm^{-2}, depending on the process.

With the heating-power densities of 1–2 W cm^{-2}, the temperature gradient over the thin (380 μm) Si wafer was shown by simulation to be small, as expected. We estimated the top carrier-surface temperature from the temperature measured on the rear side to avoid influence by the plasma. The strips had several indicator spots, which changed color once a certain temperature was reached (response time <1 s), thereby showing the maximum temperature during

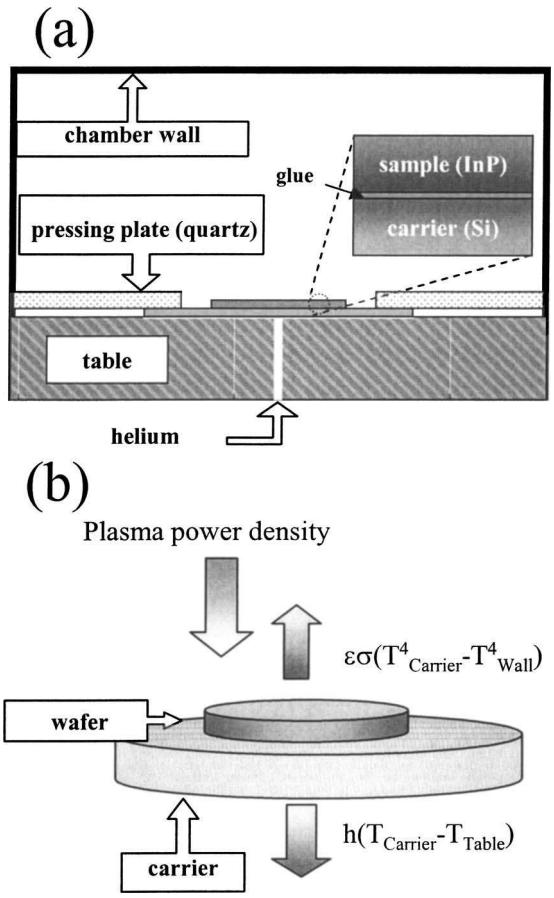

FIG. 1. (a) Schematic drawing of the parts in the ICP system considered in the heat model. (b) Schematic drawing of the inward and outward heat flux considered in the heat model. σ is the Stefan–Boltzmann constant. The Si carrier has a diameter of 102 mm and a thickness of 380 μm, the InP wafer has a diameter of 51 mm and a thickness of 350 μm, and the glue has a thickness of 100 μm.

the process. For a 1000 W Cl_2-ICP plasma with a dc-bias of 230 V for two preset table temperatures of 60 and 200 °C, the overall temperature increase amounts were 30° and 31°, with stabilization times of 30 and 20 s, respectively. In the rest of this article we estimate the real sample temperature as being 30 °C higher than the set temperature.

IV. RESULTS AND DISCUSSION

In ion-assisted chemical etching, energy barriers are locally overcome by physical bombardment so that etching can be thermally activated there. Compared to RIE and CAIBE where ion-current densities are low (<100 μA cm^{-2}), the ion bombardment in ICP can be substantial with ion-current densities up to several mA cm^{-2}. Here we investigate the thermally activated etching of different ICP processes. In particular, dry-etch results obtained at two different ICP-power/dc-bias combinations are considered: 250 W/−640 V and 1000 W/−230 V. They are referred to as processes 1 and 2, respectively. Process 1 resembles RIE etching with low ion-current density and high ion energy, while process 2 is close to an ICP mode with a relatively high ion-current density and moderate ion energy. The parameters for processes 1 and 2 are summarized in Table I.

TABLE I. Summary of process parameters and plasma properties for processes 1 and 2. To calculate the ion power density, the plasma potential as measured with the Langmuir probe was taken into account so that the acceleration voltage of the ions is not exactly equal to the measured bias voltage.

Process	ICP power (W)	Bias voltage (V)	Ion-current density (mA/cm^2)	Ion power density (W/cm^2)
1	250	−640	0.22	0.16
2	1000	−230	1.6	0.44

A. Cl_2-ICP

1. Temperature

Figure 2 shows an Arrhenius plot for processes 1 and 2 with estimated real sample temperatures. At lower temperatures, the etch rate increases slowly with temperature until it reaches 190 °C, after which a sharp increase in etch rate occurs. At this temperature, the surface is very rough (inset, Fig. 2). Above 210 °C the increase in etch rate is reduced and the etched surface is smoother (inset, Fig. 2). A similar behavior in etch rate has been observed for other Cl_2-based dry-etching processes for InP.[20,21] The rapid increase is attributed to the higher vapor pressure of $InCl_3$ at elevated temperatures.[19] The transition from a rough morphology at the onset temperature to a smoother morphology at higher temperatures relates to the differential etch rates of $InCl_3$-covered and bare InP surfaces.[24] In this narrow temperature regime, the $InCl_3$ corrosion layer is desorbed. As a consequence, the etch rate increases sharply. The activation energy ($E_A = 1.7 \pm 0.3$ eV) measured from the steep slope in Fig. 2 compares with the Arrhenius graph ($E_A = 1.7$ eV) of McNevin[19] when the etching is $InCl_3$ desorption limited. At high temperatures, the etch rate is limited by chlorine mass

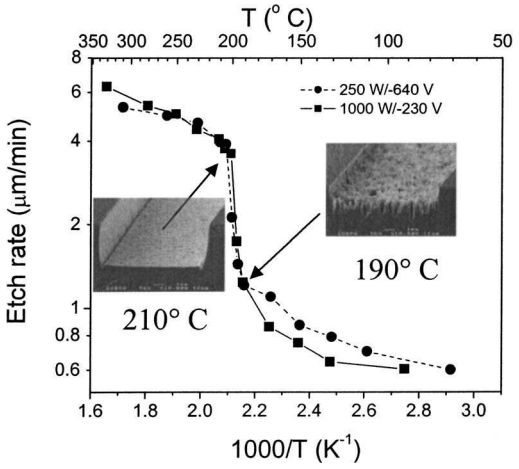

FIG. 2. Arrhenius plots of the etch rate for process 1 (250 W/−640 V) and process 2 (1000 W/−230 V). The temperatures used are the real estimated temperatures of the sample. Insert SEM micrographs show surfaces etched with process 2.

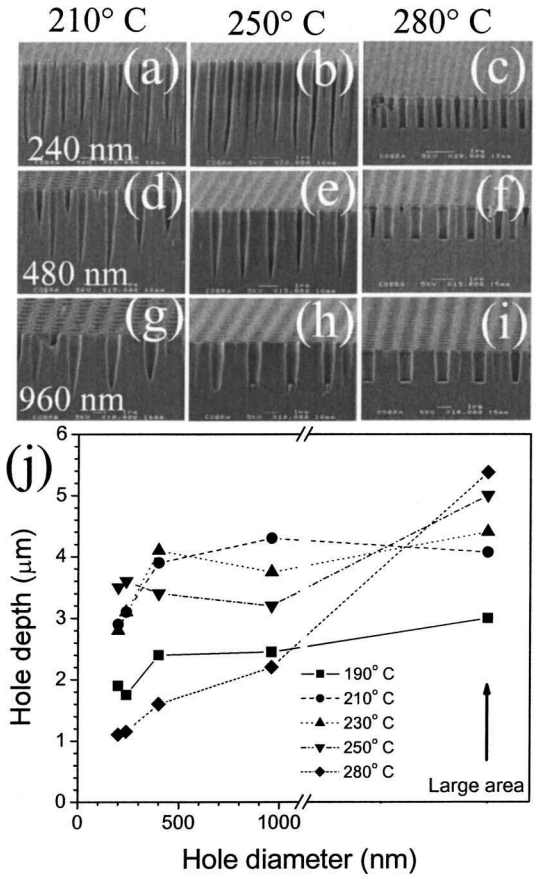

FIG. 3. [(a)–(i)] SEM micrograph of holes etched at 1.4 mtorr using process 2. The rows have the same hole diameter; the columns have the same temperature as indicated. (j) Hole depth as a function of hole diameter after etching with process 2 for 1 min at five temperatures. Temperatures refer to the real estimated sample temperature.

transport, and the increase in etch rate is lower. According to the literature, in Cl_2 vapor etching of InP at low chlorine surface coverage and at high temperatures, desorption of $InCl_3$ dominates and is probably the dominant mechanism in this regime.[24,25] The corresponding activation energies were estimated to be 0.04–0.08 eV, depending on the process, which are comparable to those reported by Sabin.[22] In the following discussion, all temperatures are presented after temperature correction, except when noted otherwise.

2. Temperature: Etching of holes

Figures 3(a)–3(i) show cross sectional SEM pictures of holes with nominal diameters of 240, 480, and 960 nm etched at 210, 250, and 280 °C with process 2 using He cooling. The holes in Fig. 3(a) are about 3 μm deep, cylindrical in the upper 1.5–2 μm, and tapered in the lower region, demonstrating that Cl_2-ICP can be used for etching deep-hole PC. At 250 °C [Fig. 3(b)], the holes exhibit some bowing in the uppermost region while the lower part is tapered. At 280 °C [Fig. 3(c)], the bowing is more pronounced. Numerical simulations made by Marcos and Rhallabi suggested that bowing results from ions scattered on the mask edge.[26] The observed temperature dependence of bowing would then suggest that the bowing etching mechanism is an ion-assisted chemical etching. In contrast to lower temperatures, the holes obtained at 280 °C [Figs. 3(c), 3(f), and 3(i)] are less deep, but wider, and have cylindrical shapes in their lower region. The increased width at 280 °C compared to lower temperatures points to a stronger chemical component.

The following model could explain the difference in shape and depth. At lower temperatures (190–250 °C), the etching is predominantly ion assisted. Shadowing of the ion flux by sidewall results in less surface activation in the corners compared to the center at the bottom of the hole. The etch rate is therefore higher there, and tapered sidewalls result. Ions scattered on the tapered walls may cause trenching, as can be observed in Fig. 3(h). For narrower holes, trenching regions touch each other and virtually disappear. The flat bottoms obtained at 280 °C indicate that there is sufficient surface activation close to the sidewalls. Therefore, the etch rate is governed by the amount of chlorine available (mass limited regime) and not limited by the ion bombardment. A part of the chlorine is consumed in the upper region due to lateral etching and, consequently, reduces the chlorine available at the bottom.

The depth dependence on hole diameter is summarized in Fig. 3(j). At 190–230 °C there is only a marginal difference in depth depending on hole diameters, except for the smallest holes that are less deep. The latter is probably due to the shadowing of ions, with the angle of incidence deviating from the surface normal, and possibly to redeposition. The flat behavior illustrates the dominance of the ion bombardment. The larger depths at 210–230 °C compared to 190 °C may be attributed to enhanced ion-assisted chemical activation. By contrast, at high temperatures (280 °C) the holes with smallest diameters are less deep than the larger holes and large areas. This suggests depletion of neutrals as the primary cause of the RIE lag in our process.[8] At 250 °C the etch behavior is in between the two regimes. On the one hand, one observes the onset of the RIE lag with large-area etch rates higher than those of the holes. On the other hand, the etch behavior in the holes is ion assisted, but with a complex balance between ion and radical fluxes changing for different hole diameters. As for the ions, there are the different ion-scattering events, depending on the hole diameter. As for the radicals, it is the Knudsen transport. As a subtle feature, the complex balance variation might point to a slight inverse RIE lag at 250 °C.

In summary, there appears to be two different etching mechanisms involved. One case is at lower temperatures (190–230 °C), where the (vertical) ion bombardment is rate limiting with a negligible RIE lag. In the other case (>250 °C) the chemical-surface activation is dominant with a significant RIE lag [Fig. 3(j)] due to limitations in material transport in high-aspect-ratio holes. We conclude that a deep photonic crystal can be etched with pure Cl_2-ICP but only in a narrow temperature range (sample temperatures of 210–230 °C).

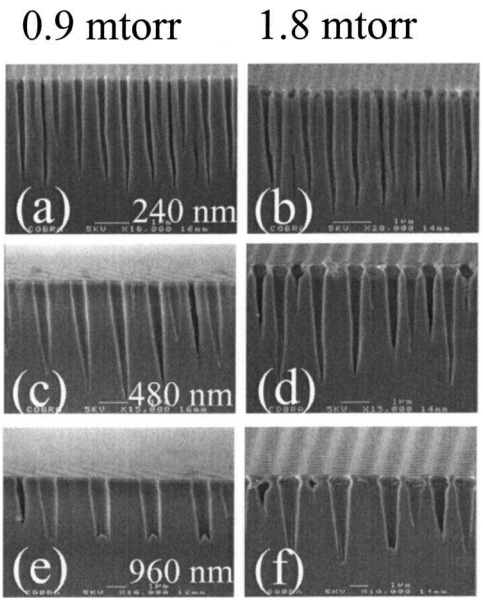

FIG. 4. SEM micrograph of holes etched at 200 °C. The hole diameters and pressures are indicated in the graph.

3. Pressure

Figures 4(a)–4(f) show the influence of pressure on hole shape for different hole diameters. The holes were etched with process 2 for 1 min at 230 °C. At the lower pressure (0.9 mtorr) all holes are conical, except for some lateral etching present in the upper region [Figs. 4(a), 4(c), and 4(e)]. The largest holes [Fig. 4(e)] exhibit trenching in the bottom, indicating significant ion bombardment. At 1.8 mtorr [Figs. 4(b), 4(d), and 4(f)], the holes are also conical but with severe lateral etching in the uppermost region. The depths of the high-aspect-ratio holes [Figs. 4(b) and 4(d)] are comparable to those obtained at the lowest pressure [Figs. 4(a) and 4(c)]. In contrast, the larger holes [Fig. 4(f)] are deeper and show only a little trenching. Further increase in pressure (>2 mtorr; results are not shown) yields shallow holes with conical shape and rough surface; the planar surface is also rough. The smallest holes suffer from a complete breakdown in their upper part to the neighboring holes.

A possible explanation for the above results is the following. At high pressure (>2 mtorr), the ion current is reduced as measured in separate runs with the Langmuir probe. Therefore, ion bombardment is insufficient to fully remove the $InCl_3$ corrosion layer. Consequently, the etch rate is low and the surface is rough. At low pressure (<2 mtorr), the ion-current density is not changed appreciably, but the supply of chlorine is low. For holes, the supply of neutrals is further impeded by low conductance.[9] At the lowest pressure (0.9 mtorr), the supply of neutral chlorine is limited for all holes, and the etching is like reactive ion beam etching where both chemical and physical (sputtering) etching occur. Sidewall scattering results in trenching for the largest holes [Fig. 4(e)]. For the smaller holes [Figs. 4(a) and 4(c)] the tapered walls are steeper, and there is no visible trenching. This indicates that ions scattered on the sidewall either hit the opposite sidewall, reducing the trenching, or hit the center region, causing etching. Since a larger area of the sidewall of the 480-nm-wide holes is exposed to the ion bombardment compared to the 240-nm-wide holes, more sidewall scattering of ions occurs. Therefore the 480-nm-wide holes are deeper. At a higher pressure (1.8 mtorr), more neutrals are available and ion-assisted chemical etching is promoted, especially inside the larger holes [Fig. 4(f)] due to their relatively low aspect ratio. Therefore, the large holes are deeper. The narrower holes are not changed appreciably at lower pressures [Figs. 4(a) and 4(b)] since there is little change in ion-current density. Another implication of an increased pressure is the reduction of the mean free path; i.e., more ions collide in the plasma sheath. Some of the colliding ions impact on the sidewall at the top of the holes, causing lateral etching there [Figs. 4(b), 4(d), and 4(f)].

A more detailed picture of the influence of pressure (and so the important balance of neutrals versus ions) on the hole shape of the important upper region is presented in Fig. 5. The best result was obtained at a chamber pressure of 1.1 mtorr [Fig. 5(a)], with holes being almost cylindrical in the upper 1–1.5 μm. The chlorine partial pressure was 1.05 mtorr due to the relatively low He leak rate. Repeating the process at a higher chamber pressure (1.4 mtorr), but a comparable chlorine partial pressure (1.1 mtorr) due to a higher He leak rate), resulted in significant barreling and tapered sidewalls, as can be observed in Fig. 5(b). This indicates that the total pressure is responsible for the difference in shape due to the change in mean free path. The mean free path for Cl_2 in the two Cl_2/He mixtures was calculated to be 30 and 20 mm, respectively, neglecting any dissociation due to the plasma. While this is large compared to the plasma-sheath thickness, which was estimated from the Langmuir probe experiment to be about 3 mm, it still means that there are 50% more collisions in the sheath at higher pressures. On the other hand, repeating the process at similar chamber pressures (1.0 and 1.2 mtorr), but with lower chlorine partial pressure (0.95 mtorr in both cases), produced holes with barreling and tapered sidewalls [Figs. 5(c) and 5(d)]. Since He by itself is not likely to be responsible for the undercut, neither by physical nor chemical etching as it is very light and inert, it is argued that vertical etching is extremely sensitive to both chamber and partial chlorine pressure. It is here speculated that for a certain chlorine partial pressure, a thick enough $InCl_x$ passivating layer is formed on the sidewall. However, if the chamber pressure is high, the number of ions hitting the sidewall is also high due to collisions in the sheath, and ion-assisted etching of the passivation layer occurs.

4. ICP power and dc bias

The above discussion on photonic-crystal etching with respect to temperature and pressure is focused on process 2. However, experiments were also performed with process 1, i.e., RIE-like etching. Here, we only mention that it is possible to etch deep photonic-crystal holes at 200 °C, while at

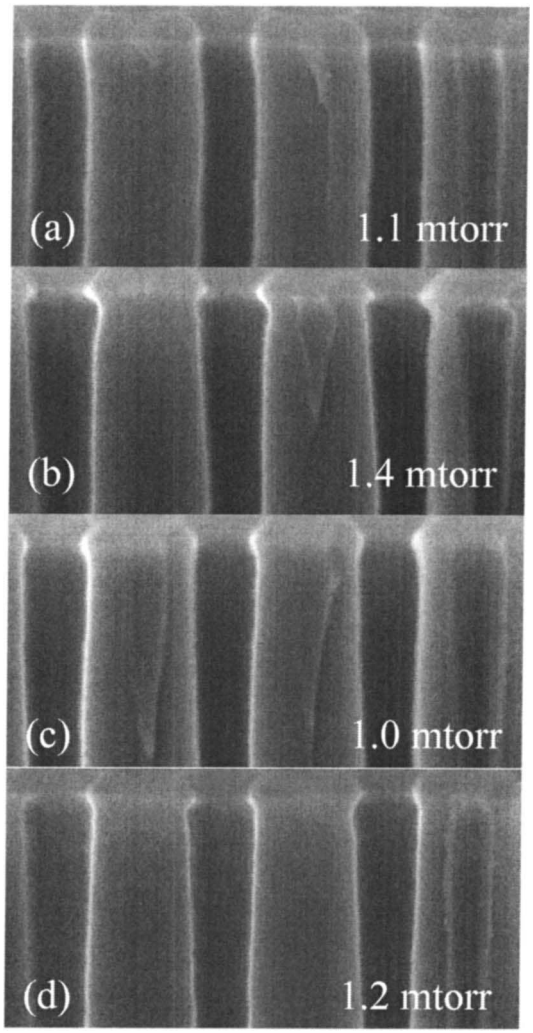

FIG. 5. SEM micrograph of holes with 240 nm diameter etched into InP at 200 °C at a total pressure and chlorine partial pressure of (a) 1.1 and 1.05 mtorr, (b) 1.4 and 1.1 mtorr, (c) 1.0 and 0.95 mtorr, and (d) 1.2 and 0.95 mtorr.

a high temperature (250 °C), lateral etching similar to process 2 is observed. It could be that the hole shape is less sensitive to pressure for other ICP/dc-bias combinations such as processes 1 and 2. This was not explored, however.

In summary, Cl_2-ICP etching of deep photonic crystals is possible in a narrow window in the temperature/pressure space. Unfortunately, the critical role of He cooling may cause substantial fluctuation in chlorine partial pressure since the He leak rate cannot be controlled. Therefore, the reproducibility is low.

B. Passivation processes

Sidewall passivation has previously been used in dry etching of pillar-type Si-based 2D-PCs. This was achieved by controlling the flux of O_2 to a SF_6 etching plasma.[27] It was shown that, in that case, the lateral etching is inhibited by the formation of an oxygen-rich reaction layer on the sidewall with a thickness of less than a nanometer.[28] On the bottom surface, this layer is removed by the ion bombardment. Here

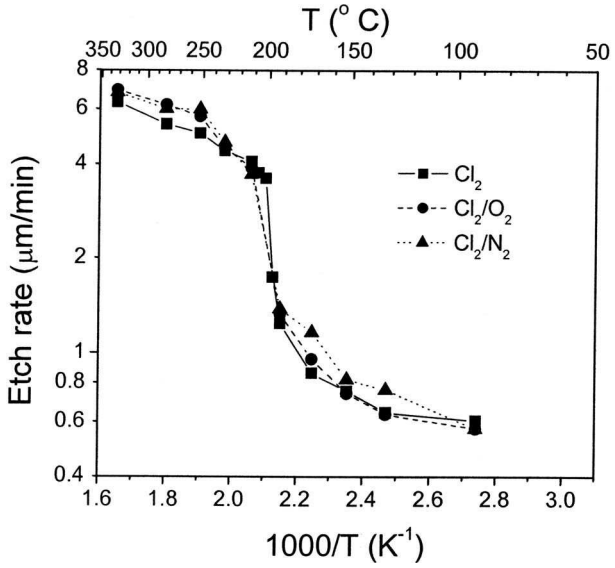

FIG. 6. Arrhenius plots of the etch rate as a function of the estimated sample temperature for different gas combinations of process 2: 14 SCCM Cl_2, 14/3 SCCM Cl_2/O_2, and 14/2 SCCM Cl_2/N_2.

we compare passivation processes based on the addition of O_2 or N_2 to Cl_2-ICP etching of InP using the same ICP system (Oxford Plasmalab 100) with He cooling. Due to limited pumping speed, the chamber pressure was kept constant at 1.4 mtorr to ensure that pressure could be maintained after the addition of the passivation gas. Operating at higher pressure levels always resulted in severe bowing and underetching of the holes in the top region.

1. Temperature and flow

The sample-temperature dependence of the large-area etch rate for process 2 with the addition of either 3 SCCM (SCCM denotes cubic centimeter per minute at STP) O_2 or 2 SCCM N_2 to the 14 SCCM Cl_2 is shown in the Arrhenius plot in Fig. 6. The etch-rate dependence of the processes with O_2 or N_2 is similar to the pure Cl_2 process shown in Fig. 2. As in that case, the strong T-dependence near 200 °C is attributed to the thermally activated desorption of $InCl_3$. However, at high temperatures, the etch rate of both passivation processes is slightly higher (Fig. 6) than that for pure Cl_2.

Much larger impact of the addition of N_2 or O_2 is manifested in high-aspect-ratio etching, such as for photonic crystal structures. A comparison of the performance of Cl_2, Cl_2/O_2, and Cl_2/N_2 processes for these structures is shown in Figs. 7(a)–7(c), respectively. The addition of a small flow (4 or 3 SCCM, respectively) of either O_2 or N_2 produces deep (~3 μm) holes with only weak barreling. Clearly, the passivation processes allow for deep hole etching at temperatures where Cl_2-ICP exhibits substantial lateral etching near the mask, which consequently reduces the Cl flux deeper into the hole.

As a consequence, the RIE lag behavior also changes drastically. Figures 8(a) and 8(b) show lag curves of holes

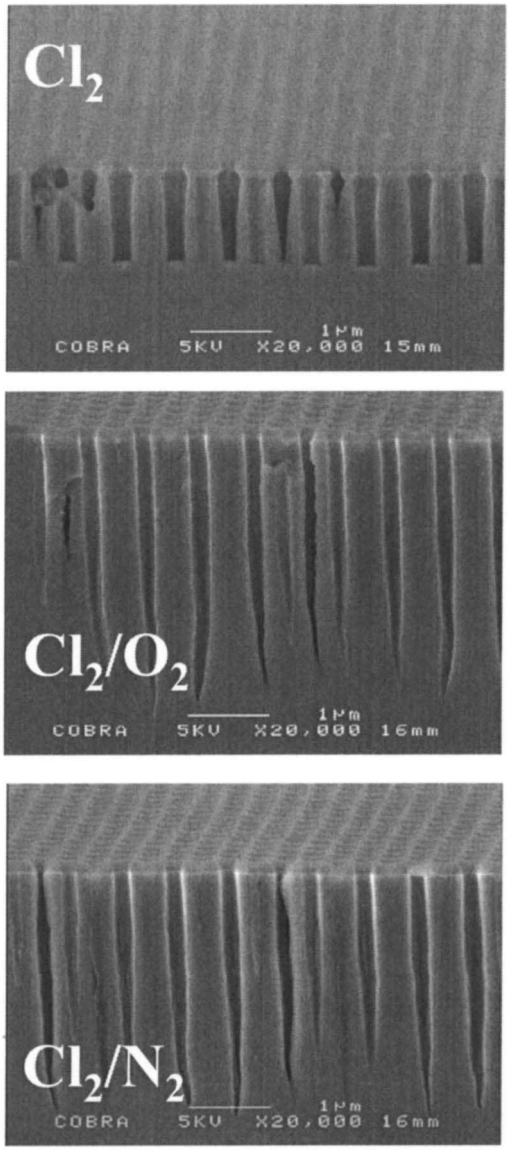

FIG. 7. SEM micrograph of 200-nm-wide holes etched with process 2 into InP at 280 °C using (a) 14 SCCM Cl_2, (b) 14/4 SCCM Cl_2/O_2, and 14/3 SCCM Cl_2/N_2.

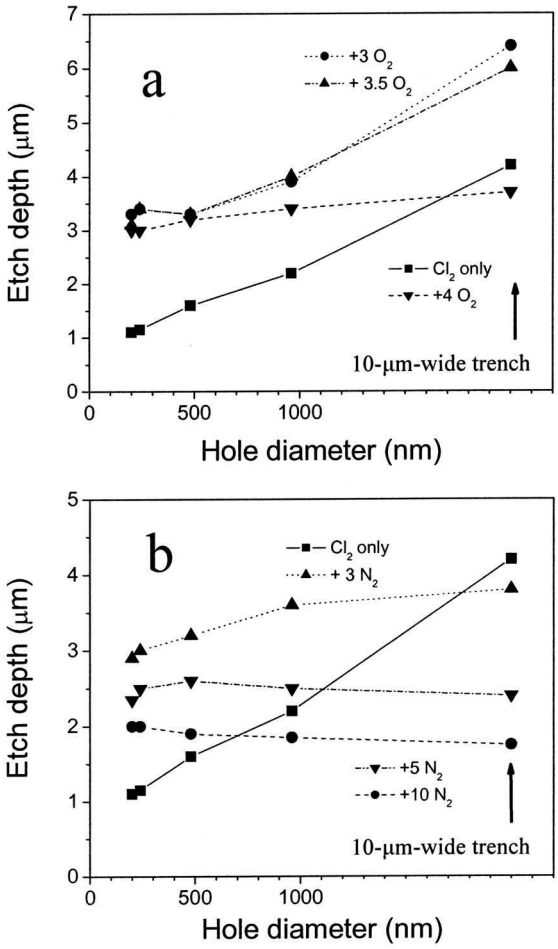

FIG. 8. Hole depth as a function of hole diameter after etching with process 2 for 1 min at 280 °C using a mixture with 14 SCCM Cl_2 and different flows as indicated for (a) O_2 and (b) N_2.

etched at 280 °C for different O_2 [Fig. 8(a)] and N_2 [Fig. 8(b)] flows. The RIE lag behavior ranges from aspect-ratio-dependent etching at low $O_2(N_2)$ concentration, where etch depth decreases with decreasing hole diameter, to aspect-ratio-independent etching at a higher $O_2(N_2)$ concentration. The smallest holes remained deep at further increases in O_2 concentration, while, in contrast, the holes of the Cl_2/N_2 process become less deep upon N_2 concentration increase. The reason for this is not yet understood. It is here speculated that the micromasking in the N_2 processes is mainly due to nitridation by ions rather than neutrals. The presence of neutrals deep inside the holes is limited by vacuum conduction, which is not the case for the ions. Optimization of the hole shape for process 2 with respect to O_2 flow and temperature was performed and yielded best results at 240 °C with 3 SCCM O_2. Higher O_2 or N_2 flow components induce heavy micromasking both in large areas and in hole structures, even at base plate temperatures as high as 250 °C.

2. ICP power and dc bias

Since the results for deep holes are ultimately limited by mask selectivity (defined as the relation between etch rates of InP and SiN_x), the residual-nitride mask thickness and the hole depth were estimated from SEM data for a wide range of ICP-power/dc-bias combinations using a 14/2 SCCM Cl_2/O_2 gas flow mixture. To optimize selectivity (large InP etch rate), a very high temperature was chosen, i.e., 250 °C set on a base plate without He cooling. The estimated sample temperature was around 300 °C. In the range of process 2, i.e., high ICP power and low dc bias, despite the selectivity being high (>15), the process at this high temperature is not useful because of severe lateral etching of the holes. However, in the range of process 1 (low ICP power, high dc bias), similar selectivities are found without substantial underetching. As shown in Fig. 9, it was possible to etch 4.5-μm-deep holes with 200 nm diameters under such conditions. The process turned out not to give smooth straight sidewalls for large-area mesas, which is a disadvantage in cases where

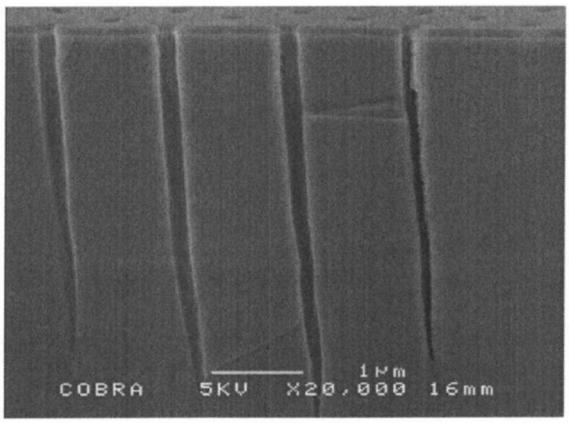

FIG. 9. SEM micrograph of 200-nm-wide holes etched for 2 min into InP at a set temperature of 250 °C without He cooling with 14/2 SCCM Cl_2/O_2 at 1.4 mtorr. The ICP power and dc bias were 250 W and 390 V, respectively.

ridge waveguides need to be etched in the same process. Also, the higher bias could be a drawback in terms of plasma-induced material damage.

An important observation is that the hole depth does not change appreciably with temperature over a large temperature range for a fixed ICP/dc-bias combination. An example is presented in Fig. 10, which shows 240 nm holes etched for 1 min with Cl_2/O_2 using 1000 W ICP power at a set temperature of 200 °C (left) and at a set temperature of 250 °C (right). The dc biases are 80 V (top) and 230 V (bottom). Temperatures refer to set temperatures here since the actual sample temperature was not estimated at a bias voltage of 80 V. The depths are comparable for a constant dc bias at the two different temperatures; however, it is less deep at 80 V than at 230 V. Apparently, in this temperature range, ion bombardment has a strong influence on the hole etch rate up to a point after which the etch rate is not further increased. Considering the results from Murrell *et al.*,[29] which suggested that ion bombardment promotes the formation of $InCl_x$, together with our observation that the hole etch rate is

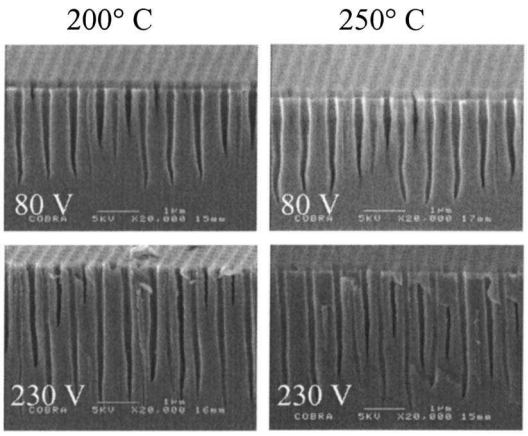

FIG. 10. SEM micrograph of 240-nm-wide holes etched into InP at 1.4 mtorr using 1000 W ICP power and Cl_2/O_2. The dc-bias voltage and set temperatures are indicated.

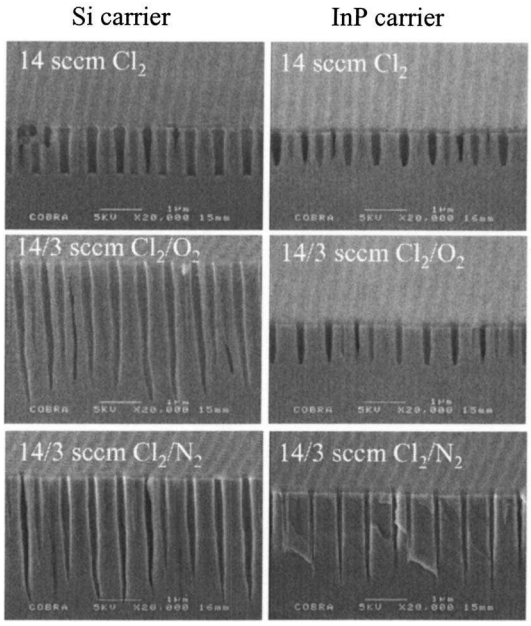

FIG. 11. SEM micrograph of 200-nm-wide holes etched into InP with process 2 at 280 °C and 1.4 mtorr. The carrier was either Si (left column) or InP (right column). Gas flows were pure Cl_2, a Cl_2/O_2 mixture, and a Cl_2/N_2 mixture with flows as indicated.

strongly dependent on the ions at weak ion bombardment and only exhibits little influence by temperature, it appears that the formation of $InCl_x$ is a rate-limiting step. When ion bombardment is strong, both the formation and the desorption rate of the $InCl_x$ are high, and the etching of the holes is mass limited (in this temperature range). This observation, in combination with the observed time independence of the hole-etch rate, suggests that a significant part of chlorine is provided by the ions. If this conclusion stands correct, it precludes the use of standard Cl_2-RIE for the etching of high-aspect-ratio holes in InP since the ion-current densities are low.

3. InP vs Si carrier

It has been observed that using a Si carrier wafer for Cl_2-ICP etching of InP will involve $SiCl_4$ as the etching species.[30,31] Similarly, from an InP carrier one may expect PCl_3 gas to participate in the etching process. Therefore, to elucidate the impact of the carrier on etching, experiments were performed with both Si and InP carriers. The etch rate of the Si carrier was measured for process 2 and found to be low (<400 nm/min) relative to the InP carrier (2.1 μm/min). While this implies that only a small fraction of the gas phase consists of Si-containing species, it does not preclude that it has any effect on etching or passivation.

Results are shown for 200 nm holes in Fig. 11. The samples were etched with process 2 for 1 min at a sample temperature of 280 °C using the three different chemistries: Cl_2 only (top), Cl_2/O_2 (middle), and Cl_2/N_2 (bottom) on InP (left) and Si carrier (right). From the SEM pictures, we observe the following: (1) The InP carrier causes a severe plasma-loading effect with hole etch rates significantly lower

than those with the Si carrier. Apparently an etch rate of the InP carrier of 2.1 μm/min is likely to deplete the chlorine content in the plasma. In contrast, more chlorine is available for the etching of the InP holes with a Si carrier. In general, it gives higher etch rates for holes compared to the InP carrier. (2) Lateral etching is observed in both cases with Cl_2 only. The bowing in the Si carrier experiments seems larger, possibly a consequence of the surplus of Cl species. (3) Sidewall passivation is obtained with both carriers and for both passivation processes. It confirms the sidewall passivation to be caused by either oxidation or nitridation of the InP with little or no involvement by $SiCl_x$ species.

The passivation effect of the Cl_2/O_2 process using the InP carrier appears to be stronger than that when using the Si carrier (Fig. 11). This is most likely because the loading effectively changes the Cl/O concentration at the surface. The holes etched with Cl_2/N_2 using the InP carrier are deeper than their Cl_2 and Cl_2/O_2 counterparts (Fig. 11). This is attributed to the micromasking that occurred on the carrier, resulting in a higher amount of chlorine available for the etching of the holes.

V. CONCLUSION

Deep photonic crystal hole structures can be etched with pure Cl_2-ICP, but only with precise control of the sample temperature and process pressure. The temperature control requires He backside cooling, which may alter the critical chlorine partial pressure due to leaking He. The addition of N_2 or O_2 for sidewall passivation makes the photonic-crystal etching process much less temperature sensitive. The large-area etch rate of the Cl_2/O_2 and Cl_2/N_2 processes are thermally activated, much like their Cl_2-ICP counterpart, which suggests that the etching mechanisms are similar. The etching should occur at sample temperatures near 200 °C where the large-area etch rate is mass limited; however, the etch rate of the holes is still ion dominated. Deep-hole etching is possible for a wide range of ICP/rf-power combinations, but the best selectivity is obtained at low ICP and low rf power. The results from the experiments using both Si and InP carriers indicate that the sidewall passivation is intrinsic to the reaction between the Cl_2/O_2- or the Cl_2/N_2-plasma and the InP.

ACKNOWLEDGMENTS

The authors would like to thank E. J. Geluk and P. Nouwens for technical assistance. Part of this research is supported by NanoNed, a technology program of the Dutch Ministry of Economic Affairs.

[1]R. Ferrini, R. Houdré, H. Benisty, M. Qiu, and J. Moosburger, J. Opt. Soc. Am. B **20**, 469 (2003).
[2]R. Ferrini, B. Lombardet, B. Wild, and R. Houdré, Appl. Phys. Lett. **82**, 1009 (2003).
[3]R. Khare, J. Brown, M. Hu, D. Pierson, M. Melendes, and C. Constantine, J. Vac. Sci. Technol. B **12**, 2947 (1994).
[4]K. K. Kho and S. W. Pang, J. Electrochem. Soc. **142**, 3945 (1995).
[5]S. Thomas III and S. W. Pang, J. Vac. Sci. Technol. B **14**, 4119 (1996).
[6]S. L. Rommel *et al.*, J. Vac. Sci. Technol. B **20**, 1327 (2002).
[7]F. Ying, W. H. Juan, and S. W. Pang, J. Vac. Sci. Technol. B **15**, 665 (1997).
[8]R. A. Gottscho and C. W. Jurgensen, J. Vac. Sci. Technol. B **10**, 2133 (1992).
[9]J. W. Coburn and H. F. Winters, Appl. Phys. Lett. **55**, 2730 (1989).
[10]M. Mulot, S. Anand, R. Ferrini, B. Wild, R. Houdré, J. Moosburger, and A. Forchel, J. Vac. Sci. Technol. B **22**, 707 (2004).
[11]M. V. Kotlyar, T. Karle, M. D. Settle, L. O'Faolain, and T. F. Krauss, Appl. Phys. Lett. **84**, 3588 (2004).
[12]A. Berrier, M. Mulot, S. Anand, A. Talneau, R. Ferrini, and R. Houdre, J. Vac. Sci. Technol. B **25**, 1 (2007).
[13]T. D. Happ, A. Markard, M. Kamp, A. Forchel, S. Anand, J. L. Gentner, and N. Bouadma, J. Vac. Sci. Technol. B **19**, 2775 (2001).
[14]F. Pommereau *et al.*, J. Appl. Phys. **95**, 2242 (2004).
[15]C. F. Carlström *et al.*, Proc. 17th International Conference on Indium Phosphide and Related Materials, Glasgow, United Kingdom, 8–12 May 2005, p. 114.
[16]R. van der Heijden *et al.*, Proc. 17th International Conference on Indium Phosphide and Related Materials, Glasgow, United Kingdom, 8–12 May 2005, p. 210.
[17]C. F. Carlström, R. van der Heijden, F. Karouta, R. W. van der Heijden, E. van der Drift, and H. W. M. Salemink, J. Vac. Sci. Technol. B **24**, L6 (2006).
[18]P. Strasser, R. Wüest, F. Robin, D. Erni, and H. Jäckel, J. Vac. Sci. Technol. B **25**, 387 (2007).
[19]S. C. McNevin, J. Vac. Sci. Technol. B **4**, 1216 (1986).
[20]N. DeMeo, J. P. Donnelly, F. J. O'Donnell, M. W. Geis, and K. J. O'Connor, Nucl. Instrum. Methods Phys. Res. B **7–8**, 814 (1985).
[21]C. Youtsey, R. Grundbacher, R. Panepucci, I. Adesida, and C. Caneau, J. Vac. Sci. Technol. B **12**, 3317 (1994).
[22]E. Sabin, J. Vac. Sci. Technol. B **16**, 1841 (1998).
[23]http://www.dowcorning.com/applications/search/default.aspx?R=104EN
[24]M. Vernon, T. R. Hayes, and V. M. Donelly, J. Vac. Sci. Technol. A **10**, 3499 (1992).
[25]A. Jenichen and C. Engler, Surf. Sci. **561**, 171 (2004).
[26]G. Marcos and A. Rhallabi, J. Vac. Sci. Technol. A **21**, 87 (2002).
[27]T. Zijlstra, E. van der Drift, M. J. A. de Dood, E. Snoeks, and A. Polman, J. Vac. Sci. Technol. B **17**, 2734 (1999).
[28]M. Blauw, Ph.D. thesis, Delft University of Technology, 2004.
[29]A. J. Murrell, R. J. Price, R. B. Jackman, and J. S. Foord, Surf. Sci. **227**, 197 (1990).
[30]A. Matsutani, H. Ohtsuki, F. Koyama, and K. Iga, Jpn. J. Appl. Phys., Part 1 **39**, 6109 (2000).
[31]A. Matsutani, H. Ohtsuki, S. Muta, F. Koyama, and K. Iga, Jpn. J. Appl. Phys., Part 1 **40**, 1528 (2001).